DOI: 10.13009/EUCASS2017-615

Modification of Spacecraft Materials under Electron Radiation

Elena Plis, Daniel P. Engelhart**, Russell Cooper***, Ryan S. Booth****, Dale Ferguson***, Ryan Hoffmann****

**Assurance Technology Corporation*

84 South Street, Carlisle, MA 01741, USA

***National Research Council Fellow at Air Force Research Laboratory*

Kirtland AFB, Albuquerque, NM, USA

**** Air Force Research Laboratory, Space Vehicles Directorate*

Kirtland AFB, Albuquerque NM, USA

*****Institute for Scientific Research, Boston College*

Chestnut Hill, MA 02467

Abstract

In the presented work, we studied the alterations of optical properties and electrical conductivity of polyimide (PI) that had been irradiated by an electron dose similar to that of Geosynchronous Earth Orbit (GEO) - like environment. We correlate these material properties to the underlying chemical changes that occur in PI. Several complimentary characterization techniques were utilized to qualify and quantify radiation induced chemical changes in the material, including the directional-hemispherical reflectance (DHR) technique coupled with IR absorption/reflection spectroscopy and dark resistivity measurements.

1. Introduction

Polyimide (PI) films, in particular, Kapton-H®, are extensively used in the spacecraft industry for applications involving thermal and electrostatic control [1-4]. Spacecraft materials on orbit are subjected to the harsh effects of space weather, including hard vacuum, atomic oxygen, ultraviolet light, charged particle radiation, etc. [5,6] causing degradation of their optical and physical properties [7,8]. It is important to understand the alterations of spacecraft materials' properties induced by the space environment to improve satellite lifetime, system reliability, space situational awareness, and to decrease satellite operational and construction costs. The change of PIs' material properties under simulated space environments, including surface degradation [9-11], mechanical properties [12,13], conductivity [14], and absorptivity [15], has attracted the attention of researchers however, the relation of these radiation-induced changes to the chemical nature of damage still needs to be investigated.

In general, it has been found that the space environment fundamentally changes spacecraft materials [e.g. 16-18]. The nature of particles primarily responsible for damage is dependent on the orbit; in GEO this is high energy electrons. The damage induced by an incident flux of high energy particles proceeds via two different mechanisms of particle energy loss: ballistic and electronic. Damage which can be described by the interaction of highly energetic atomic nuclei with atomic nuclei in the polymer (ballistic term) involves rupture of every bond within a certain radius of the particle's pathway through the polymer due to the massive amounts of energy deposited over very short distances upon impact. The damage described by interactions of incident electrons with electrons in the polymer (electronic term) results in electronic excitation leading to selective bond breakage and radical formation. Electronic damage pathways are expected to be bond-specific, i.e. the weakest bonds will be ruptured preferentially. When the polymer is bombarded with high energy electrons, it is reasonable to expect that the electronic damage mechanism will be more prevalent than the ballistic due to the negligible mass of electrons.

The electronic damage mechanism is one of simultaneous kinetic processes taking place during and immediately after material irradiation with high energy electrons. Other processes include healing (formation of bonds identical to those damaged, returning the material to its pristine state) and scarring (formation of new chemical bonds in the damaged material which are different from those in the pristine material). Often macroscopic properties are being measured, making it difficult to distinguish healing from scarring; hence, we refer to the sum of healing and scarring as recovery. Understanding these processes will allow development of a predictive model for materials' optical and transport properties as a function of exposure to the space environment.

DOI: 10.13009/EUCASS2017-615

In the presented paper, we first characterized the change of optical and charge transport properties that occur in PI when it is exposed to high energy electrons. Several complimentary optical and electrical characterization techniques were utilized to qualify and quantify radiation induced chemical changes in the material, including the directional-hemispherical reflectance (DHR) technique coupled with IR absorption/reflection spectroscopy, and charge-discharge measurements. Next, we attempted to understand the nature of radiation-induced chemical modifications that drive the degradation of the physical properties.

2. Experimental

Space weather at GEO is a combination of high vacuum, electron (0.01 – 10 MeV) and proton (10^{-4} – 10 MeV) fluxes, solar radiation, and thermocycling between 120–150 K and 400–420 K [19]. In order to understand the interaction of each component of the space environment with a material, it is necessary to characterize these effects individually. Moreover, in terms of total dose experienced by an object in GEO over several solar cycles, electrons are the dominant source of energy deposition.

For simulation of an electron dose typical for GEO environment, PI samples were bombarded with high energy (90 keV) mono-energetic electron radiation from a Kimball Physics EG8105-UD electron flood gun in the Spacecraft Charging and Instrument Calibration Laboratory (SCICL) at Kirtland Air Force Base in New Mexico, USA [20]. In order to accurately characterize the electron dose profile a Monte-Carlo simulation of energy loss per unit length was performed with the Monte Carlo N-Particle Code, v. 6.1 (MCNP6.1) [21]. In this simulation, 20 million 90 keV electrons impinged on a 76 μm thick Kapton film backed by an aluminum layer of infinite thickness. The simulation results presented in Figure 1 show the average energy deposition per electron per 1 μm thick Kapton layer. Backscattering and bremsstrahlung were also accounted for in the simulation. According to the simulation, the average energy deposited per electron per μm is 1.08 keV.

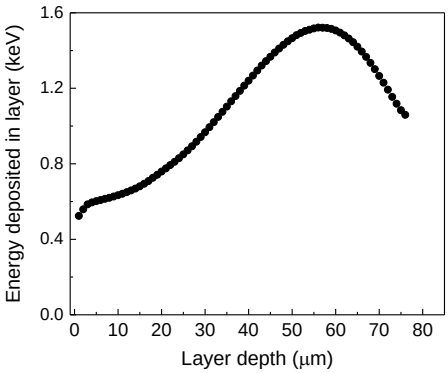

Figure 1: Energy deposited in 76 μm Kapton by 90 keV electron beam

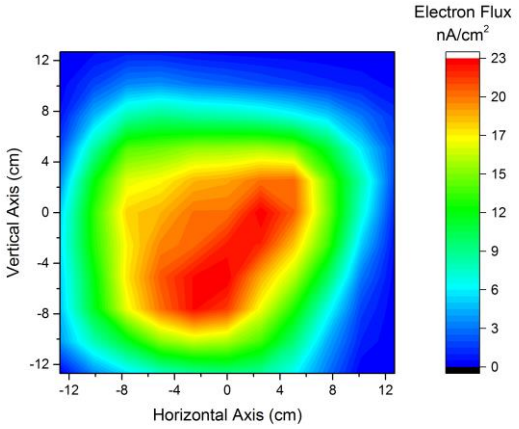

Figure 2: Beam map of 90 keV electron beam

Prior to the radiation exposure, the 90 keV electron beam was characterized via a Faraday cup mounted *in situ* [20]. The resulting beam map is presented in Figure 2. Average electron flux received by PI film during irradiation was 7.8 nA/cm^2. To ensure uniformity of the irradiation dose, PI sample was mounted on a rotating grounded aluminum carousel. A 24 hour vacuum dehydration bake was performed on PI film at 60°C prior to radiation exposure. PI used in this study was irradiated with several doses, as listed in Table 1, without breaking the vacuum.

The volume resistivity of irradiated samples was measured *in vacuo* with a TREK 10 kV high speed electrostatic voltmeter model using the surface potential decay (SPD) method [22]. After every irradiation experiment, the electron flux was turned off, and surface potential decay curve was measured with the non-contact voltmeter positioned 1-2 mm from the sample's surface. After the front of the charge body has migrated through the material and has reached the grounded carousel, the dissipation of charge is primarily determined by the loss of electrons from the material. PI was mounted on grounded aluminium carousel with stainless steel clamps. SPD measurements were performed in darkness to eliminate the possibility of optically excited states obscuring our analysis.

DOI: 10.13009/EUCASS2017-615

Table 1: Summary of irradiation experiments

Experiment ID	Dose Gy	Dose years of equivalent GEO exposure
1	16.6 x 10^6	2.5
2	33.6 x 10^6	4.9
3	53.6 x 10^6	7.9
4	73.3 x 10^6	10.8

Once the damaged material, irradiated with a total cumulative dose of 73.3 x 10^6 Gy, was evacuated from the vacuum chamber under nitrogen exposure, it was placed into a smaller vacuum chamber for SPD measurements, in order to quantify the effect of short air exposure (7 minutes) during material transfer from two vacuum chambers on the charge transport characteristics of the irradiated material. Surface potential discharge characteristics of damaged PI were assessed and compared with those of pristine material using low-energy (5 keV) Kimball Physics EGPS-2017B electron gun and TREK probe model 370 high speed electrostatic voltmeter.

The optical properties of PI radiation-damaged with the highest dose, 73.3 x 10^6 Gy, were measured during the recovery process with visible and near infrared (VNIR) absorption/reflection spectroscopy and the DHR method, performed with Perkin-Elmer Lambda 950 UV/VIS Spectrometer (0.4 – 2.5 μm) and Surface Optics Corporation SOC-400T portable FTIR spectrometer (2 – 25 μm), respectively. FTIR spectroscopy probes chemical bonding by exciting vibrational transitions within the polymer. Because every chemical bond has unique vibrational energy states, measuring which wavelengths of IR light are absorbed provides highly specific chemical information. This technique provides information on the molecular bonding environment, chain conformation, and orientation of specific functional groups of pristine, damaged, and recovered materials. Changes in the position and intensity of the IR absorption "fingerprint" of damaged and recovered materials offer further insights into what chemical bonds are being modified during the radiation-induced degradation and recovery process.

Due to the complex PI structure, its IR spectrum is also complex and difficult to interpret. The simulation of Kapton-H pristine and irradiated IR spectra was performed using the M06 functional and the 6-31g(d,p) basis set on a Kapton dimer with the Gaussian 09 Software Package [23] to help the interpretation of IR data. The dimer consisted of the correct endcaps if the polymerization reaction were to only occur between two Kapton monomers. Energies for bond breakages were performed by optimizing the geometry of the reactant and the two resulting products after the bond fission assuming homolytic cleavage (i.e. one electron goes with each of the products resulting in a pair doublet spin states). The energy is then calculated by subtracting the sum of the products from the reactants. For example, the dissociation of OH thus, [OH→O+H]: ΔE_{rxn}= [E(O)+E(H)]-E(OH). Isomerization products were optimized and then the energy of the optimized structure was subtracted from the reactant. Harmonic frequencies were calculated from the minimized structures and scaled by 0.96 throughout the paper for comparison to experimental data. All calculations were run using the DoD High Performance Computing Modernization Program.

3. Results

Using the SPD method, the dark resistivity of the material may be derived from a plot of surface potential versus time, hereafter referred to as a decay curve [24]. A representative surface potential decay curve is shown in Figure 3. The post-transit region is indicated by the red line and represents the time it takes electrons deposited from the beam to traverse the material and be lost to the grounded backing plate. This region of the decay curve is fitted by Eq. 1, from which the dark resistivity of the material is derived

$$V_s(\tau_{decay}) = m\tau_{decay}^b$$
$$\rho_{dark} = \frac{\tau_{decay}}{\epsilon_0 \epsilon_r} \quad (1)$$

DOI: 10.13009/EUCASS2017-615

where τ_{decay} is charge decay time in seconds; m and b are fitting parameters; ε_0 and ε_r are the permittivity of free space and relative permittivity of the PI material, respectively. Conductivity of the material is then calculated as inversely proportional to the resistivity of the material, as presented in Figure 4.

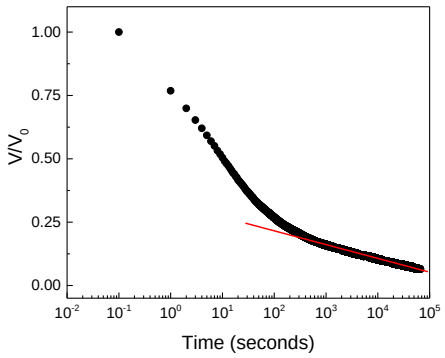

Figure 3: Representative SPD curve. Red line indicates the fit from which resistivity is derived

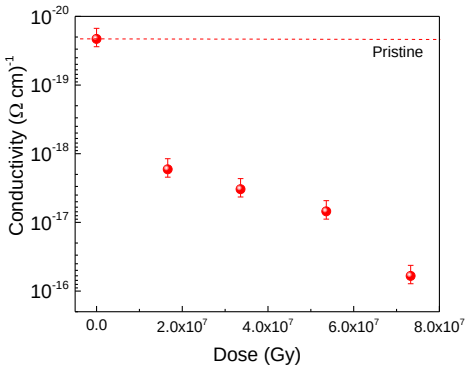

Figure 4: Conductivity of PI material irradiated with different doses

SPD measurements performed on the PI irradiated with a cumulative dose of 73.3 x 10^6 Gy after short (less than 5 minutes) air exposure resulted in a resistivity of 2.8 x 10^{17} ± 8.5 x 10^{15} Ω·cm and conductivity of 3.5 x 10^{-18} ± 9.6 x 10^{-20} 1/ Ω·cm. The latter value is an order of magnitude lower than the conductivity of the same sample measured under vacuum, 6.0 x 10^{-17} ± 1.8 x 10^{-17} 1/ Ω·cm, suggesting the degrading effect of an air exposure on the irradiated material characteristics.

The effect of an air exposure on the optical properties of irradiated material is evident from the transmittance spectra of radiation-damaged PI measured during air recovery process, as presented in Figure 5. A decrease in the optical bandgap was observed for the radiation damaged material which tends to return to nearly that of the pristine material with increased air exposure.

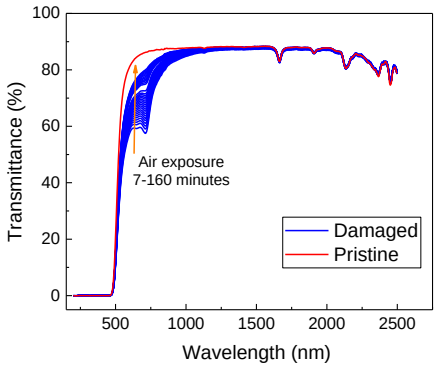

Figure 5: Transmittance spectra of pristine PI sample and radiation damaged film measured during air recovery process.

To eliminate the deleterious effect of air exposure on the analysis of irradiated PI, prior to FTIR measurements it was placed into portable vacuum chamber, hereafter referred to as a vacuum wallet, as depicted in Figure 6. It features a spring-loaded plunger with a gold mirror which ensures a good contact between the irradiated PI sample and the CaF_2 window. The sample is mounted at the center of the device in a differentially pumped vacuum chamber.

The IR spectrum of a pristine Kapton-H sample measured with the vacuum wallet device is presented in Figure 7. Several characteristic vibration assignments were identified using the existing body of literature [25-28] and summarized in Table 2.

DOI: 10.13009/EUCASS2017-615

(a) (b)

Figure 6: Vacuum wallet (a) before and (b) after loading of irradiated PI sample

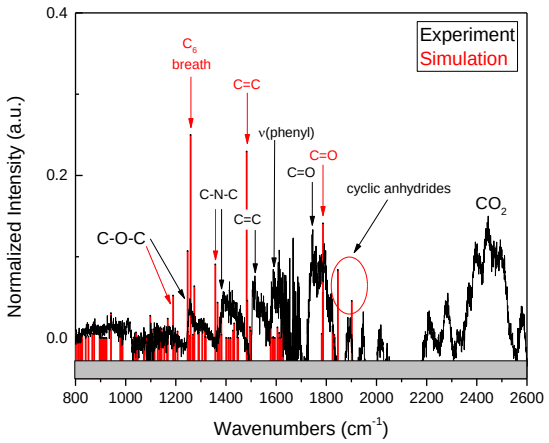

Figure 7: Experimental and simulated IR spectra of pristine PI. Some characteristic vibration assignments are identified

Table 2: Vibrational assignments of pristine Kapton-H

Assignment	**Absorption** (cm^{-1})		**Characterization**
	Simulated pristine	Experimental pristine	
ν(C-O-C)	1195	1263	Bridging C-O-C stretch
C_6	1258	-	C_6 breath coupled with C_6H_4 wag
δ(C-N-C)	1362	1380	Imide stretch
C=C	1481	1515	Aromatic C=C stretching
ν(phenyl)	1607	1598	Phenyl ring C-C stretch
ν(C=O)	1790	1746	Out-of-phase carbonyl stretch
Cyclic anhydride	1849 1903	1825 1889	Cyclic anhydrides, presented in not fully cured polymer (precurser)
CO_2	-	~2400	CO_2 absorption

DOI: 10.13009/EUCASS2017-615

Normalized IR absorbance spectra of PI material irradiated with cumulative dose of 73.3 x 10^6 Gy and a pristine Kapton-H sample measured with the vacuum wallet are presented in Figure 8. Figure 9 shows the experimental and simulated IR spectra of damaged PI. Characteristic vibrational assignments are summarized in Table 3.

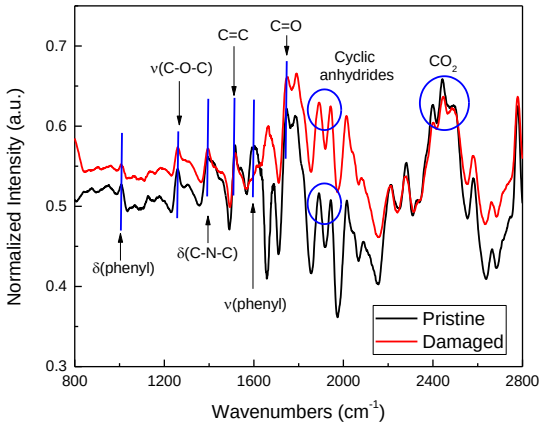

Figure 8: Normalized IR absorbance spectra of PI material irradiated with cumulative dose of 73.3 x 10^6 Gy and pristine Kapton-H sample measured with vacuum wallet device. Some characteristic vibration assignments are identified.

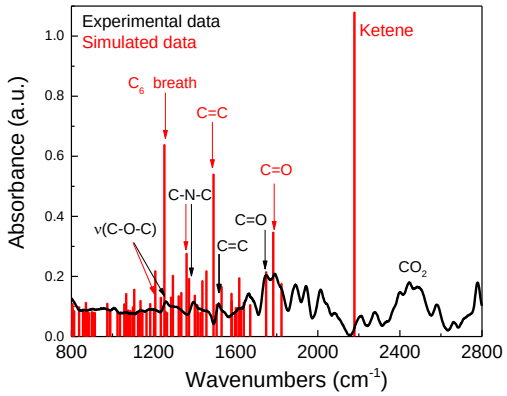

Figure 9: Experimental and simulated IR spectra of damage PI. Some characteristic vibration assignments are identified.

Table 3: Vibrational assignments of damaged and pristine Kapton-H

Assignment	**Absorption** (cm^{-1})			**Characterization**
	Pristine experimental	Damaged experimental	Simulated damaged	
δ(phenyl)	1004	1006	-	Phenyl ring deformation
C_6	-	-	1258	C_6 breath coupled with C_6H_4 wag
ν(C-O-C)	1263	1261	1195	Bridging C-O-C stretch
δ(C-N-C)	1380	1390	1362	Imide stretch
C=C	1515	1515	1481	Aromatic C=C stretching
ν(phenyl)	1598	-	1607	Phenyl ring C-C stretch
ν(C=O)	1746	1749	1790	Out-of-phase carbonyl stretch
Cyclic anhydride	1890-1940	1890-1940	1850	Cyclic anhydrides, presented in not fully cured polymer
C=C=O	-	-	2198	Ketene
CO_2	~2400	~2400	-	CO_2 absorption

4. Discussion

The conductivity of electron-irradiated PI changed significantly compared to pristine film. The conductivity of radiation-damaged PI showed an increase of two orders of magnitude after irradiation with an initial dose, 16.6 x 10^6

DOI: 10.13009/EUCASS2017-615

Gy, and further increases for larger doses, as shown in Figure 4. Charge transport in disordered materials, like PI, occurs via incoherent hopping among transport sites. Bulk conductivity is influenced by both energetic and geometric disorder. That is to say, the facility with which an electron can travel through a disordered material in the presence of a strong electric field is dependent on both the energetic distribution of transport sites within the material and the geometric distribution of the transport sites. The latter dependency arises due to the variation of intersite electronic wavefunction overlap arising from the positional and orientational distribution of these hopping sites [29]. We attribute the dose-dependent bulk conductivity increase in irradiated PI to the radiation-induced formation of electron hopping sites, created as a result of bond-specific rupture during electron bombardment, which are not present in the pristine material. This phenomenon is distinct from radiation induced conductivity which is temporary and is the result of increased energy in the system and not modification of the transport sites within the material as seen here.

Formation of radiation-induced electronic states is confirmed by the UV/Vis transmission measurements. Transmission spectra presented in Figure 5 indicate a red shift of the absorption edge, or an effective shrinking of the PI's "band gap" to ~1.8 eV in the damaged material due to the emergence of radiation-induced electronic states. Compared to the measured "band gap" of pristine Kapton of 2.3 eV [30], these states are energetically shallow and act as additional electron hopping sites, thus increasing the conductivity of the damaged material.

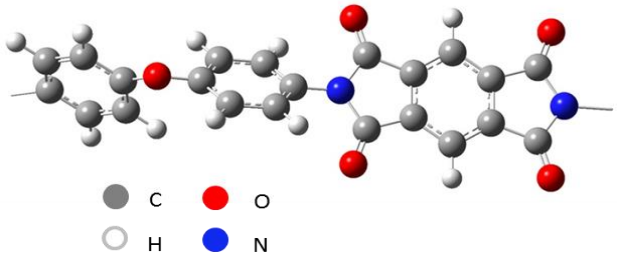

Figure 10: Schematic of polyimide monomer

For demonstrative ease of analysis of IR data, a schematic of the PI monomer is shown in Figure 10.

A comparison of the experimentally taken IR spectrum of pristine Kapton with a simulated IR spectrum for the same material is shown in Figure 7. Several interesting dependencies were found. First, in the measured IR data, the out-of-phase carbonyl stretch ν(C=O) peak is red-shifted with respect to its assignment in simulated IR spectrum, from 1746 cm^{-1} to 1790 cm^{-1}, respectively. This may be attributed to intermolecular hydrogen bonding between the CO and neighbouring polymers. Next, the absorption peak corresponding to bridging C-O-C stretch, ν(C-O-C), is found at 1263 cm^{-1} and it overlaps with the C_6 breath assignment of the simulated spectrum. The C_6 breath absorption is not observed in experimentally taken IR spectrum of pristine Kapton. The mode corresponding to the C_6 breathing mode coupled with the C_6H_4 wags on the benzyl ether group. This vibration is not observed in the experimental IR spectra at the calculated frequency and intensity due to perturbations in the solid phase not present in the gas phase calculations.

Finally, aromatic C=C stretching (~ 1500 cm^{-1}) and phenyl ring C-C stretch (~ 1600 cm^{-1}) absorption frequencies match very closely in both experimental and simulated IR spectra. It should be noted that absorption features at ~ 1850 cm^{-1} and ~ 1890 cm^{-1}, correspond to cyclic anhydrides present in the precursor molecules and the incompletely cured polymer. These cyclic anhydrides were deliberately used as the endcaps in the simulated IR spectrum and these peaks correlate well with our experimental data. The large absorption peak at ~ 2400 cm^{-1} falls beyond the well-characterized (400-2000) cm^{-1} region. We attribute absorption feature at ~ 2400 cm^{-1} to the CO_2 atmospheric absorption [31].

Comparison of the IR spectra of damaged and pristine PI in Figure 8 reveals two interesting radiation-induced changes in the IR fingerprint of the damaged film. First, the absorption at the wavelength associated with the carbonyl (C=O, 1746 cm^{-1}, 1749 cm^{-1}) out-of-phase stretch increased after electron bombardment. This suggests first that existing carbonyl moieties were not preferentially broken due to electron bombardment. A significant reduction in the absorption associated with phenyl ring C-C stretch (1598 cm^{-1}) after electron bombardment suggests that ether breakage is accompanied by rupture of the phenyl rings in the monomer, possibly leading to the formation of a new pi-bonded carbon structure containing the new carbonyl.

DOI: 10.13009/EUCASS2017-615

Comparison of the measured IR spectrum of radiation-damaged Kapton with the simulated IR spectrum for the same material is shown in Figure 8. Several identified absorption frequencies are similar to those of the pristine film, for both the experimentally measured and simulated spectra. The main difference is the presence of a C=C=O group, ketene, in simulated IR spectrum. The calculated IR absorption spectrum of the pristine polymer is generated from a DFT simulation of a PI dimer with one end terminating in an anhydride moiety and the other end an amine, corresponding to the chemical structures of the chemical precursors. The IR absorption spectrum of the "damaged" PI is generated from a DFT calculation of a molecule consisting of a complete PI monomer with an amine endcap on one end and the other (imide) end bonded to a ketene (C=C=O) type structure meant to represent the result of ether breakage, phenyl ring rupture, and the formation of a carbonyl like structure bonded to a newly formed cyclic C_4NO structure resulting from the bonding of the ruptured phenyl with one carbonyl of the imide. This structure was envisioned as a chemical pathway which is consistent with our FTIR data. DFT calculations suggest that the ring structure is more stable (by 31.2 kcal/mol) than a simple pi-bonded ketene structure. As is clearly shown in Figure 9, the resulting absorption peak is not present in the measured spectrum indicating that this structure is not formed under electron bombardment with enough frequency to be detected via our IR spectroscopy experiments or that the resulting structure is not IR active. Furthermore, since the calculated “damaged” PI structure was optimized under gas phase conditions and the experimental FTIR data was performed on solid phase PI, it is likely that if the ketene group exists it is involved with the neighbouring PI chains. This may lead to cross linking or other intermolecular interactions which perturb the calculated “ideal” C=C=O geometry and electron distributions resulting in shifts in both frequency and intensity of the calculated gas phase frequency when compared to the experimental IR spectra.

5. Conclusions

We have investigated optical and charge transport properties of PI irradiated with high-energy electrons similar to those presented in GEO environment with optical absorption spectroscopy and surface potential decay measurements. Electron bombardment of PI induces chemically specific bond rupture. As a result, PI becomes very reactive and sensitive to its surrounding atmosphere, causing dramatic and unwanted effects. As an example of such effects, transmission of irradiated PI changed from 57% to 82% (at 720 nm) during 160 min of air exposure, as shown in Figure 5. In our previous work we also demonstrated the deleterious effect of even limited (less than 10 minutes) air exposure on charge carrier transport in irradiated material [32].

To exclude the effect of air exposure on charge transport properties of radiation-damaged material, the dose-dependent bulk resistivities were measured *in vacuo*, whereas IR absorption spectra were accessed using a vacuum wallet device, which limited atmospheric exposure to less than a minute.

Analysis of IR spectrum of irradiated PI suggests formation of new chemical structures originating from a radiation-induced brakeage of phenyl rings and/or ether bridges forming a metastable carbonyl. These new chemical structures give rise to new, lower energy electronic states than are present in the pristine material as demonstrated by a red-shift in the absorption edge of the material. Then the dose-dependent bulk conductivity increase in irradiated PI may be attributed to the formation of electron hopping sites, created as a result of bond-specific rupture during electron bombardment.

6. Acknowledgements

We would like to acknowledge support from the Air Force Office of Scientific Research, Aerospace Materials for Extreme Environments (Dr. Ali Sayir) and Remote Sensing and Imaging Physics (Dr. Stacy Williams) programs. Grants 17RVCOR401 and 17RVCOR414.

References

[1] X. Qiu, Y. R. Zhou, Z. Shen. 2016. Electrical Properties of ITO/Kapton/Al Anti-Static Thermal Control Coating in Space Radiation Environments. *Int. J. Simulat. Syst. Sci. Tech.* 17:1-4.

[2] J. Arenberg, J. Flynn, A. Cohen, R. Lynch, J. Cooper. 2016. Status of the JWST sunshield and spacecraft. *Proc. SPIE* 9904: 990405-990410.

DOI: 10.13009/EUCASS2017-615

[3] A. F. Holland, J. Pearson, W. Lysford, J. Straub. 2016. Consideration of the use of origami-style solar panels for use on a terrestrial/orbital wireless power generation and transmission spacecraft. *Proc. SPIE* 9865: 98650E.
[4] C. Ham and K.-C. Lin. 2016. Study of a Gossamer sail and its application to LEO spacecraft for space debris mitigation and attitude control. *FAE* 5: 38-48.
[5] K. L. Bedingfield, R. D. Leach, M. B. Alexander. 1996. NASA Reference Publication 1390.
[6] D. C. Ferguson, S. P. Worden, D. E. Hastings. 2015. The Space Weather Threat to Situational Awareness, Communications, and Positioning Systems. *IEEE Trans. Plasma Sci.* 43 (9), 3086-3098.
[7] J. A. Dever, S. K. Miller, E. A. Sechkar, T. N. Wittberg. 2008. Space Environment Exposure of Polymer Films on the Materials International Space Station Experiment: Results from MISSE 1 and MISSE 2. *High Perform. Polym.* 20: 371-387.
[8] R. K. Kiefer, W. J. Gabler, M. T. Hovery, and S. A. Thibeault. 2011. The effects of exposure in space on two high-performance polymers. *Radiat. Phys. Chem*. 80 (2): 126-129.
[9] F. Awajaa, J. B. Moon, M. Gilbert, S. Zhang, C. G. Kim, and P. J. Pigram.2011. Surface molecular degradation of selected high performance polymer composites under low earth orbit environmental conditions. *Polym. Degrad. Stab*. 96 (7): 1301-1309.
[10] R. Verker, N. Atar, F. Quero, S.J. Eichhorn, E. Grossman. 2013. Tensile stress effect on the macromolecular orientation and erosion mechanism of an atomic oxygen irradiated polyimide. *Polym. Degrad. Stab.* 98(5): 997-1005.
[11] X. Lei, M. Qiao, L. Tian, Y. Chen, Q. Zhang. 2015. Evolution of surface chemistry and morphology of hyperbranched polysiloxane polyimides in simulated atomic oxygen environment. *Corros. Sci.* 98: 560-572.
[12] H. Shimamura and T. Nakamura. 2010. Investigation of degradation mechanisms in mechanical properties of polyimide films exposed to a low earth orbit environment. *Polym. Degrad. Stab*. 95 (1): 21-33.
[13] Z. Shen, Y. Mu, Y. Ding, Y. Liu, C. Zhao. 2015. Study on the mechanical property of polyimide film in space radiation environments. *Proc. SPIE* 9796: 97960U.
[14] R. Hanna, T. Paulmier, P. Molinie, M. Belhaj, B. Dirassen, D. Payan, N. Balcon. 2014. Radiation induced conductivity in space dielectric materials. *Appl. Phys.* 115:033713.
[15] C. P. Ennis and R. I. Kaiser. 2010. Mechanistical studies on the electron-induced degradation of polymethylmethacrylate and Kapton. *Phys. Chem. Chem. Phys.* 12: 14902-14915.
[16] Y. Wu, C. Sun, J. Xiao, R. Li, D. Yang, S. He. 2010. A study on the free-radical evolution and its correlation with the optical degradation of 170 keV proton-irradiated polyimide. *Polym. Degrad. Stab*. 95 (7): 1219-1225.
[17] Y. M. Sun, Z. Y. Zhu, Y. F. Jin, C. L. Liu, Z. G. Wang. 2002. The effects of high electronic energy loss on the chemical modification of polyimide. Nucl. Instr. Meth. Phys. Res. B 193: 214-220.
[18] D. P. Engelhart, E. Plis, S. Humagain, S. Greenbaum, D. Ferguson, R. Cooper, R. Hoffmann. 2016. Chemical and Electrical Dynamics of Polyimide Film Damaged by Electron Radiation. In: *14th Spacecraft Charging Technology Conference*.
[19] J.-C. Mateo-Velez, A. Sicard-Piet, D. Lazaro, V. Inguimbert, P. Sarrailh, S. Hess, V. Maget, and D. Payan. Severe Geostationary Environments: Numerical Estimation of Spacecraft Surface Charging from Flight Data. 2016. *J Spacecr Rockets* 53: 304-316.
[20] R. Cooper and R. Hoffmann. 2015. Jumbo Space Environment Simulation and Spacecraft Charging Chamber Characterization. Air Force Report No. AFRL-RV-PS-TP-2015-0012, Air Force Research Laboratory, Albuquerque, New Mexico, USA.
[21] J.T. Goorley. 2014. MCNP6.1.1-Beta Release Notes. LA-UR-14-24680.
[22] A. R. Frederickson and J. Dennison. 2003. Measurement of conductivity and charge storage in insulators related to spacecraft charging. *IEEE Trans. Nucl. Sci.* 50(6): 2284-2291.
[23] Frisch, M. J.; Trucks, G. W.; Schlegel, H. B.; Scuseria, G. E.; Robb, M. A.; Cheeseman, J. R.; Scalmani, G.; Barone, V.; Mennucci, B.; Petersson, G. A.; et al. Gaussian 09, Revision E.01; Gaussian, Inc: Wallingford, CT, 2009.
[24] J. R. Dennison, J. Brunson, P. Swaminathan, N. W. Green, and A. R. Frederickson. 2006. Methods for High Resistivity Measurements Related to Spacecraft-Charging. *IEEE T PLASMA SCI* 34: 2191-2203.
[25] R. Nurmukhametov, D. Y. Likhachev, S. Lavrov, and J. Y. Kardash. 1989. Features of electronic absorption spectra of aromatic polyimides and polyisoimides. *POLYM SCI USSR* 31: 434-440.
[26] E. Ortelli, F. Geiger, T. Lippert, and A. Wokaun 2001. Pyrolysis of Kapton® in air: an in situ DRIFT study. *APPL SPECTROSC* 55: 412-419.
[27] R. Li, C. Li, S. He, M. Di, and D. Yang. 2008. Damage effect of keV proton irradiation on aluminized Kapton film. *RADIAT PHYS CHEM* 77: 482-489.
[28] T. Steckenreiter, E. Balanzat, H. Fuess, and C. Trautmann. 1999. Pyrolytic effects induced by energetic ions in polymers. *NUCL INSTRUM METH B* 151: 161-168.

DOI: 10.13009/EUCASS2017-615

[29] Y. N. Gartstein and E.M. Conwell. 1995. Off-diagonal disorder and activation-energy of high-field hopping motion. *Phys. Rev. B* 51(11): 6947-6952.
[30] Yohei Komiyama, S.S., Hiroaki Miyake, Yasuhiro Tanaka, Tatsuo Takada *Observation of Surface Discharge Phenomena on Dielectric Films Under Low Pressure Using Pockels Effect* in *Protection of Materials and Structures From the Space Environment*, M.T. Jacob Kleiman, Yugo Kimoto, Editor. 2012, Springer Verlag. p. 456.
[31] L. Li. 2011. Dielectric properties of aged polymers and nanocomposites. *Graduate Thesis and Dissertation*. Paper 12128: 52.
[32] D. P. Engelhart, E. Plis, S. Humagain, S. Greenbaum, D. Ferguson, R. Cooper, R. Hoffmann. 2016. Chemical and electrical dynamics of polyimide film damaged by electron radiation. 14th Spacecraft Charging Technology Conference, ESA/ESTEC, Noordwijk.